forests

MDPI

Article

Change in Micromechanical Behavior of Surface Densified Wood Cell Walls in Response to Superheated Steam Treatment

Elin Xiang [1], Rongfeng Huang [1,*] and Shumin Yang [2]

[1] Key Lab of Wood Science and Technology of State Forestry and Grassland Administration, Research Institute of Wood Industry, Chinese Academy of Forestry, Beijing 100091, China; xiangelin@163.com
[2] Bamboo and Rattan Science and Technology Laboratory, International Center for Bamboo and Rattan, Beijing 100102, China; yangsm@icbr.ac.cn
* Correspondence: huangrf@caf.ac.cn; Tel.: +86-010-62889451; Fax: +86-62881937

Abstract: The combination of surface densification and superheated steam treatment is an effective method to improve the mechanical properties and dimensional stability of low-density wood. The objective of the current work is to evaluate the effects of superheated steam treatment on the micromechanical behavior of surface densified wood. The microstructure, chemical composition, cellulose crystalline structure, and micromechanical behavior of surface densified wood under different superheated steam pressures were investigated. Results indicated that both 0.1 MPa and 0.3 MPa superheated steam treatments increased the elastic modulus and hardness of fiber cell walls in surface densified wood. However, the average creep ratio and maximum creep compliance J(50) of surface densified wood under 0.3 MPa decreased by 41.59% and 6.76%, respectively, compared with untreated wood. The improvement of elastic modulus, hardness and creep resistance of surface densified wood treated with superheated steam was associated with the increase of relative crystallinity (CrI) and crystalline size. In addition, 0.3 MPa superheated steam treatment displayed a better effect on the enhancement of the elastic modulus, hardness, and creep resistance of the fiber cell wall than 0.1 MPa superheated steam treatment.

Keywords: surface densified wood; superheated steam treatment (SHT); cell wall; creep behavior; nanoindentation (NI)

Citation: Xiang, E.; Huang, R.; Yang, S. Change in Micromechanical Behavior of Surface Densified Wood Cell Walls in Response to Superheated Steam Treatment. *Forests* **2021**, *12*, 693. https://doi.org/10.3390/f12060693

Academic Editor: Luis García Esteban

Received: 5 May 2021
Accepted: 25 May 2021
Published: 28 May 2021

1. Introduction

Poplar (*Populus tomentosa*), an important economic timber species widely cultivated in China, is renowned for its rapid growth, high yield, and adaptability. However, poplar wood has a lower basic-density (0.41–0.47 g/cm^3), hardness (2.90–3.45 kN), modulus of rupture (MOR) (73.9–81.2 MPa), and compressive strength perpendicular to the grain (23.0–38.0 MPa), which was lower than that of other known hardwood species such as Machurian Ash (*Fraxinus mandschurica*) and beech (*Fagus longipetiolata*) [1]. These physical and mechanical properties cannot satisfy performance requirements in many applications, such as construction, furniture, and flooring. As an effective wood modification approach, surface densification can significantly improve the physical and mechanical properties of low-density species by only compressing the first few millimeters beneath the surface under suitable moisture and temperature conditions [2–4]. Compared with bulk densification, surface densification could enhance wood availability by reducing volume loss and result in high energy efficiency [5,6].

However, densified wood without any post-treatment has poor dimensional stability and returns to its initial raw shape and size when exposed to liquid water or even high humidity environments [4,7,8]. Some attempts have been made to overcome this issue, including synthetic resin impregnation [9,10], cross-linking reaction [11,12], heat treatment [13,14], saturated steam treatment [15,16], and superheated steam treatment [16–18].

Among the various modification methods, superheated steam treatment has distinct superiority in the aspects of simple operation, low pressure-resistant requirements for equipment, cost-effectiveness, and lack of chemical additives. The compressive deformation of surface densified wood can be effectively stabilized under specific combinations of superheated steam treatment process parameters, even upon repeated exposure to moisture [17,18]. Surfaced densified wood treated with superheated steam can be used for non-structural applications, such as tabletops, solid wood flooring, and furniture, due to its excellent performance in surface hardness and dimensional stability [17]. Furthermore, it has been found that the presence of steam in the superheated steam treatment process can accelerate the transfer of heat and mass. It promotes degradation of the chemical components in the wood, resulting in a more significant change in the performance of pressurized superheated steam treatment than that of atmospheric superheated steam treatment [19]. Changes in microstructure, chemical composition, and the mechanical and physical properties [17–20] of wood treated with superheated steam have been intensely investigated.

Wood is a natural macromolecule polymer composite with cellulose, hemicelluloses, and lignin. It has the dual properties of elastic solids and viscous liquids. The deformation of wood gradually increases with time under a quasi-static load, a phenomenon called creep [21]. Creep behavior is an essential feature for evaluating the quality of wood products and the safety of the structural design. Therefore, tracking the changes of creep behavior upon superheated steam treatment is essential to ensure the safe use of surface densified wood. There are many factors affecting the creep behavior of wood, including moisture content [21,22], temperature [23], and wood structure [24,25]. Wang et al. (2002) [26] studied the impact of air heat treatment on the creep behavior of densified wood, and their results showed that the higher the treatment temperature, the higher the instantaneous compliance of the corresponding test material in the process of absolute drying or hygroscopic desorption. In addition, previous studies on the creep behavior of heat-treated wood mainly focused on the macroscopic scale and rarely reported on the sub-micrometer scale. The structure and chemical composition of the plant cell wall are some of the key factors affecting the mechanical properties of cell walls [27,28]. Understanding the specific molecular mechanical properties at cellular and subcellular levels is of great significance to understanding the modification effect of superheated steam treatment and further optimizing the process parameters of superheated steam treatment.

Nanoidentation (NI) is a powerful non-destructive testing technique to evaluate the mechanical properties of biomaterials at the sub-micrometer scale, such as elastic modulus parameters, hardness parameters, and viscoelastic properties [23,27–29]. However, studies of how superheated steam treatment affects the creep behavior of densified wood at the sub-micrometer scale have not been reported so far. The objective of this study is to evaluate the effects of superheated steam treatment on the micromechanical behavior of surface densified wood. For this purpose, changes in microstructure, chemical composition, cellulose crystalline structure, and micromechanical behavior were analyzed by means of a scanning electron microscope (SEM), Attenuated total reflectance-Fourier transform infrared (ATR-FTIR), X-ray diffraction (XRD), and NI, respectively. The Burger's model was fitted to the experimental data of creep behavior, and the viscoelastic parameters were calculated.

2. Materials and Methods

2.1. Materials

Poplar is a fast-growing hardwood species that is mainly cultivated in the alluvial plain of the middle and lower reaches of the Yellow River. Poplar has been widely used in a variety of industrial fields such as pulping, papermaking, wood-based panels, and biofuel. In this research, a 25-year-old poplar round wood was obtained from a plantation forest in Guan County, Shandong Province, China. The poplar log was sawn into lumber with dimensions of 1000 mm (L) × 110 mm (T) × 50 mm (R) and then kiln-dried to a moisture content of 9.0–12.0%. The lumber was then further processed into wood lumber specimens

with a smaller dimension of 400 mm (L) × 100 mm (T) × 25 mm (R) (Figure 1a) with an average density of 0.44 g/cm^3 (RH 65%, 20 °C).

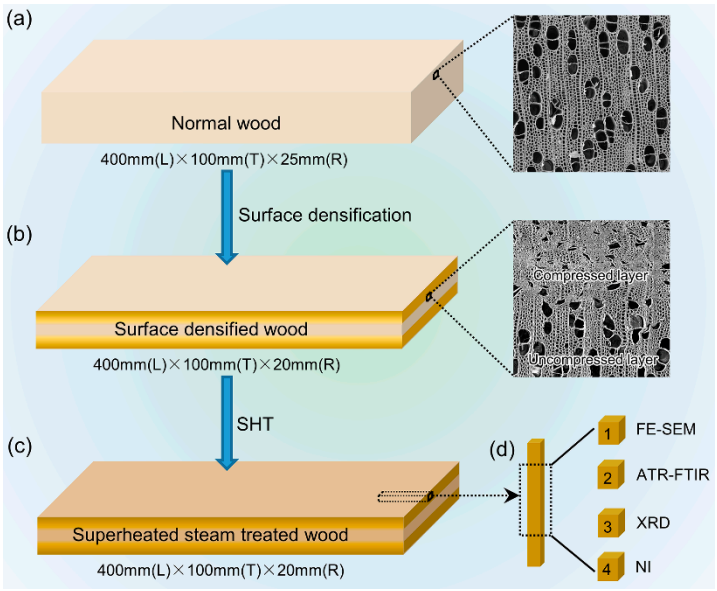

Figure 1. Schematic illustration of the preparation of surface densified wood treated with superheated steam. Normal wood (**a**), surface densified wood (**b**), surface densified wood treated with superheated steam (**c**), preparation of test specimen (**d**). SHT: superheated steam treatment.

2.2. Surface Densification and Superheated Steam Treatment (SHT) Process

Kiln-dried lumber specimens were coated with molten paraffin on the transverse sections and then immersed in deionized water at 20 °C for 2 h. The immersed specimens were preheated in an open hot-press at 165 °C for 10 s and then compressed under a loading perpendicular to the fiber axis. The target compression ratio was 20% (Figure 1b). After compressing to the target thickness, the specimens were kept under a pressure of 6 MPa and a temperature of 165 °C for 30 min. Finally, before opening the hot-press plates, the upper and lower plates were cooled down to 80 °C for 10 min. The prepared surface densified wood specimens were randomly divided into three groups, of which two were used for superheated steam treatment and one for control, with each group having three replicates of the boards. Prior to superheated steam treatment, the surface densified wood specimens were dried in an oven at 60 °C with a moisture content below 10% and then treated in a sealed tank (Xinandrying 0938) with 0.1 MPa and 0.3 MPa superheated steam at 180 °C for 2 h. The detailed process procedure for superheated steam treatment has been reported in our previous studies [18,20,30]. To minimize the differences in the specimen itself and ensure the accuracy of the indentation position, all test specimens were taken from the 15th growth ring (located on the surface of the surface densified wood) and divided into four parts according to Figure 1d.

2.3. SEM Observation

The surface morphological of surface densified wood specimens was observed using a field emission scanning electron microscope (XL30 ESEM FEG; FEI CO., Hillsboro, OR, USA) at an accelerating voltage over 7 kv.

2.4. XRD Analysis

Untreated and treated wood specimens were cut into small pieces and then ground into wood powders with a particle size between 40 and 60 mesh using a Willey mill. To analyze the effect of superheated steam treatment on the crystalline structure of cellulose, the powder was examined via an X-ray diffractometer (X' Pertpro30X) with Cu Kα radiation

(λ = 0.154 nm). The XRD pattern was determined with the following parameters: scanning range, 5–40°; voltage, 40 kV; electric current, 40 mA; and scan rate, 3°/min. Each specimen's crystallinity index (CrI) and crystal dimension were calculated according to the Segal method [31] and the Scherrer's formula [32], respectively.

$$\mathrm{CrI} = \frac{I_{002} - I_{am}}{I_{002}} \times 100\% \quad (1)$$

where CrI is relative crystallinity (%); I_{002} is the maximum intensity of the lattice diffraction angle of 002; and I_{am} is the minimum intensity corresponding to amorphous cellulose fraction.

$$D_{\mathrm{hkl}} = \frac{k\lambda}{\beta_{1/2} cos\theta} \quad (2)$$

where D is the dimension of the crystalline region (nm); k is the diffraction constant (0.89); λ is the incident wavelength (0.154); $\beta_{1/2}$ is the diffraction peak half wide (radian); and θ is the diffraction angle (°).

2.5. ATR-FTIR Analysis

Untreated and treated wood specimens were ball-milled to a fine wood powder with a mesh size of 100. ATR-FTIR spectra were collected by a Nicoleti S10 Fourier transform infrared spectrometer (Thermo Fisher Scientific Co., Waltham, MA, USA) via the KBr tablet method. Each spectrum was collected for 32 scans at a spectral resolution of 8 cm^{-1} over the wavenumber of 4000–400 cm^{-1}. The original spectra were normalized, and the baseline was corrected using OPUS 7.8 software.

2.6. NI Test

A small stick with a size of 3 (L) × 2 (T) × 2 (R) mm^3 was cut from the densified layer of the specimens. Stick specimens were dehydrated, embedded in the epoxy resin Spon 812, and trimmed at the transverse section in a Leica UC6 ultramicrotome equipped with a diamond knife. NI experiments were carried out on a Hysitron TI 950 nano-indentation meter (Hysitron Inc., Minneapolis, MN, USA) equipped with a scanning probe microscope and a diamond Berkovich tip (tip diameter is less than 100 nm) to evaluate the indentation elastic modulus, hardness, and creep behavior. Before the test, all samples were placed in a nano-indentation instrument and balanced for at least 24 h at 21 °C and 65 ± 4% relative humidity. The three-stage trapezoidal loading mode was adopted, and the loading time was 5 s, the load holding time was 50 s, and the unloading time was 5 s (Figure 2a, load-time curve). During the whole indentation test, the peak loading force was 200 μN, and an indentation depth of 100–160 nm was formed on the S2 cell wall layer of the fiber (Figure 2a, depth-time curve). To ensure the reliability of the creep results, at least 25 effective indentation measurements were conducted for each group of specimens. Four important parameters were recorded during the nano-indentation test, which were loading time, loading force, projected area A, and pressing depth h.

For the creep test, the stress remained unchanged at the holding segment, and the indentation creep rate was used to describe the relative variation of indentation depth.

$$C_i = \frac{h_2 - h_1}{h_1} \times 100 \quad (3)$$

where C_i is creep ratio; h_2 is the max penetration depth at the end of holding segment; and h_1 is the depth at the end of loading segment (Figure 2a).

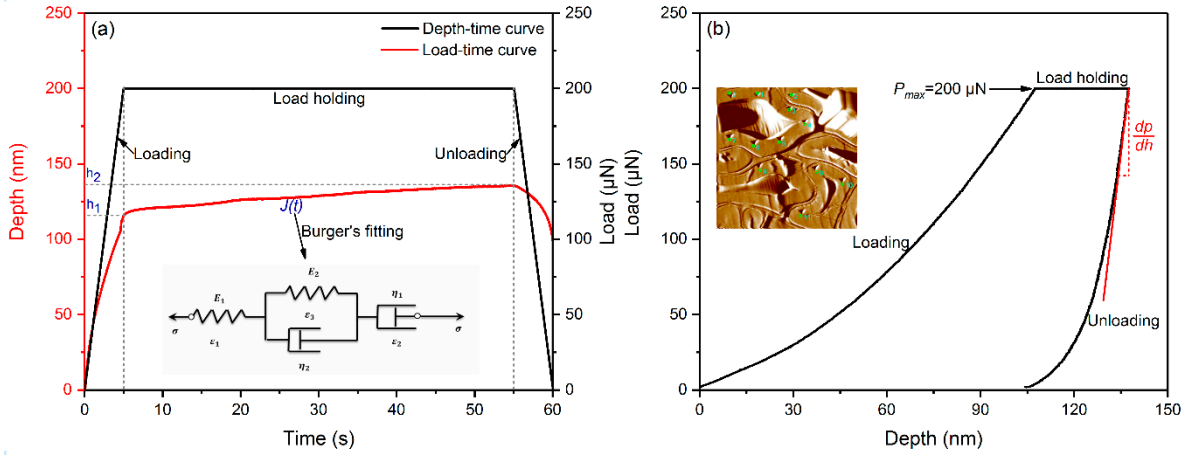

Figure 2. Schematic diagram of depth-time and load-time curve (**a**) and the corresponding indentation load-depth graph (**b**).

Based on previous literatures [21–23], the creep compliance is given by the following:

$$J(t) = \frac{A(t)}{2(1-\nu^2)P_0 \tan\delta} \quad (4)$$

where ν is the Poisson ratio of the cell wall (ν = 0.21), and δ is the half opening angle of the indenter. P_0 is the holding load. The contact area *A(t)* is greatly relevant to indentation depth and is calculated by the area function of the tip. The area function of the tip refers to previous studies by Wang et al. (2019) [22].

The experimental data of the creep test was fitted to the Burger's model, made up of four components, which comprise the association in series of the Maxwell model and Kelvin model (Figure 2a). Based on Burger's model, creep compliance can be rewritten as the following formula:

$$J(t) = J_0 + J_1 \cdot t + J_2[1 - \exp(-t/\tau_0)] \quad (5)$$

where $J_0 = \frac{1}{E_e}$; $J_1 = \frac{1}{\eta_1}$; $J_2 = \frac{1}{E_d}$; $\tau_0 = \frac{\eta_2}{E_d}$, E_e, E_d, η_1 , η_2 , τ_0 are elastic modulus, viscoelastic modulus, plasticity coefficient, viscoelastic parameter, and hysteresis time, respectively.

The elastic modulus and hardness were calculated according to the load-depth curves of Olive and Pharrs (1992) [33] (Figure 2b).

$$H = P_{max}/\mathrm{A} \quad (6)$$

where *H* is hardness (GPa); *Pmax* is the peak load determined at a maximum indentation depth in an indentation cycle; and A is the projected area of contact between the indenter and the test specimen.

$$\mathrm{Er} = \frac{\sqrt{\pi}}{2\beta}\frac{\mathrm{S}}{\sqrt{\mathrm{A}}} \quad (7)$$

where Er is the elastic modulus (GPa); S (stiffness) is the slope of the tangent line of the unloading curve in the load-depth plot; β is a correction factor related to indenter geometry (β value is 1.034 for Berkovich indenter); and A is the projected area of contact.

2.7. Statistical Analysis

Data of chemical composition, cellulose crystalline structure, elastic modulus, hardness, and creep behavior of the surface densified wood were statistically analyzed via analysis of variance (ANOVA) using the least significant difference method to determine the level of significance at $p < 0.05$.

3. Results and Discussion

3.1. Microstructure of Cell Wall

The microstructure of the transverse section of the surface densified wood with and without superheated steam treatment was visualized through SEM (Figure 3). The SEM images showed that the obvious deformation of the fiber and vessel cell wall was observed after the compression in loading perpendicular to the fiber axis at a 20% compression rate. The vessel cell cavity changed from an oval shape to flat shape, and a few fiber cell cavities were completely closed (Figure 3a,d, dotted line). After superheated steam treatment, there was no significant change in the morphology of the vessel and fiber cell wall (Figure 3b,c). However, a closer examination of the fiber cell wall at high resolutions revealed that several micro-cracks and fractures appeared on the fiber cell wall of the specimens (Figure 3e,f, arrow). This phenomenon is consistent with the results of Xing et al. (2016) [23] on the changes of the cell wall structure of *Larix gmelinii* subjected to heat treatment at 180 °C and 220 °C, respectively. Hemicelluloses, one of the least heat-resistant polymers in wood cell walls, underwent degradation during the heat treatment at 180 °C [28,34]. Based on these results, it is speculated that the appearance of micro-cracks on the fiber cell wall could be the consequence of hemicelluloses degradation during the superheated steam treatment. More gaps between the secondary wall layers of the fiber cell in 0.3 MPa superheated steam treatment wood are clearly visible with respect to 0.1 MPa superheated steam treatment (Figure 3e,f, dotted circle), indicating that the increase of superheated steam pressure may accelerate the separation of cell wall layers. Gao et al. (2019) [17] found that steam pressure had a negative impact on wood MOR. Thus, it was speculated that the change in the cell wall microstructure after superheated steam treatment might also be one reason for the decrease of MOR.

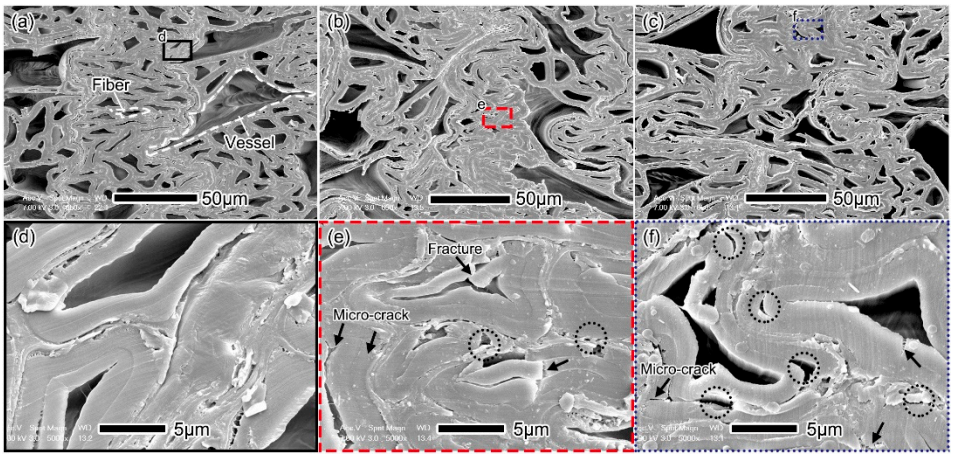

Figure 3. SEM micrographs of the transverse section of surfaced densified wood with and without superheated steam treatment. Untreated (**a**,**d**), superheated steam treatment at 0.1 MPa (**b**,**e**), and 0.3 MPa (**c**,**f**). (**d**–**f**) are enlarged images of the areas selected in (**a**–**c**) under high resolution, respectively.

3.2. Chemical Composition

The distribution and binding pattern of cellulose, hemicelluloses, and lignin in plant cell walls are a critical factor affecting macro- and micro-mechanical behavior. Figure 4a displays the ATR-FTIR spectra of surface densified wood with and without superheated steam treatment. Some changes in the intensity of the characteristic peaks could be observed at, for example, 1739 cm^{-1}, 1595 cm^{-1}, and 1505 cm^{-1}. Previous researchers have reported that the absorption peak at around 1423 cm^{-1} is assigned to the CH_2 scissor motion in cellulose and assumed to be essentially unaltered by superheated steam treatment [18] or saturated steam treatment [35,36]. Thus, this absorption band (1423 cm^{-1}) was used for spectrum normalization. Semi-quantitative results of the ratio of the intensity of the above characteristic peaks to the 1423 cm^{-1} peak are shown in Figure 4b.

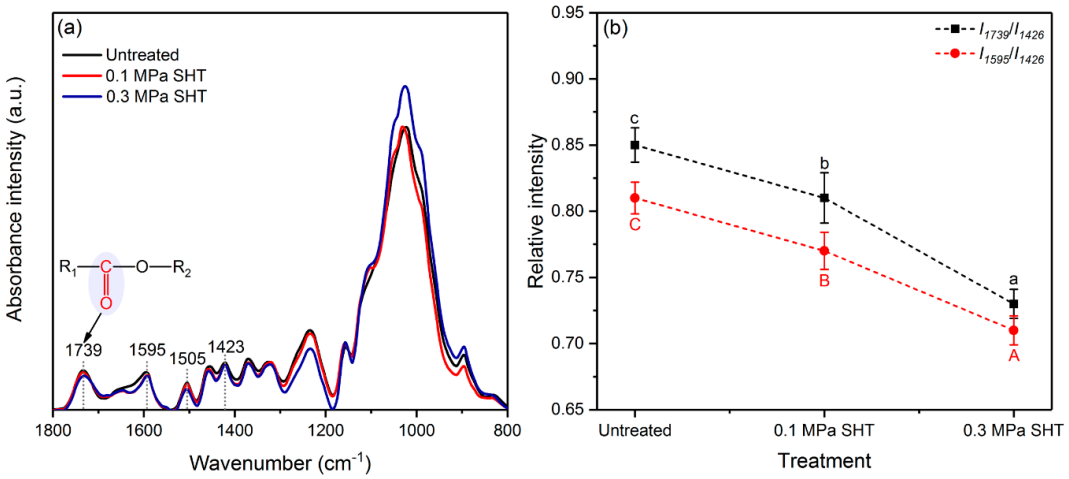

Figure 4. ATR-FTIR spectra (**a**) and the relative intensities changes of the absorption peaks at 1738 cm^{-1} and 1595 cm^{-1} (**b**) of surface densified wood with and without superheated steam treatment.

The bands near 1739 cm^{-1} correspond to C=O stretching vibrations in the O=C-OH group of xylan. Compared with the untreated wood, superheated steam treatment at 0.1 MPa and 0.3 MPa resulted in an absorbance ratio reduction of 0.04 and 0.12, respectively, indicating that deacetylation reaction occurred in hemicelluloses during the treatment. This agrees well with the findings of 180 °C heat treatment and saturated steam treatment [18,35]. ATR-FTIR absorption at 1595 cm^{-1} was ascribed to the C=O stretching vibration and aromatic skeleton vibration. The intensity of this peak is reduced after superheated steam treatment, and maximal reduction was 14.08% at 0.3 MPa superheated steam treatment. Absorbance at 1505 cm^{-1} assigned to aromatic skeleton vibration is also lower than that of untreated wood. The above changes in the peak intensity indicate that hemicelluloses and lignin structure in wood have been affected by 0.1 MPa and 0.3 MPa superheated steam pressure at 180 °C.

3.3. Cellulose Crystalline Structure

Figure 5 shows the X-ray diffraction (XRD) patterns of surface densified wood with and without superheated steam treatment. The distraction diffraction at the 2θ angles of 15.60°, 22.16°, and 34.42° correspond to (101), (002), and (040) crystal plans of cellulose, respectively [37]. Compared with the untreated wood, (002) diffraction peak of surface densified wood treated with 0.1 MPa and 0.3 MPa superheated steam is significantly enhanced, indicating that superheated steam treatment resulted in a change in the crystalline structure of cellulose in surface densified wood.

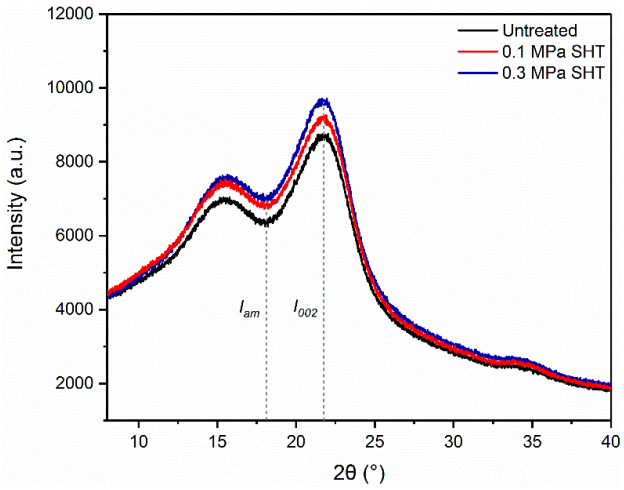

Figure 5. XRD pattern of surface densified wood with and without superheated steam treatment.

Detailed statistical results of the cellulose crystalline parameters are shown in Table 1. The CrI of surface densified wood treated with 0.1 MPa and 0.3 MPa superheated steam are 44.14% and 46.78%, respectively, which are higher than that of untreated wood. Increasing CrI correlated with the degradation of amorphous regions of cellulose during steam treatment [37,38]. After 0.1 MPa and 0.3 MPa superheated steam treatment, the crystallite thickness of cellulose increased to 3.53 nm and 3.81 nm, which are 1.56% and 6.51% higher than that of untreated wood, respectively. This agrees well with previous findings for heat-treated wood and steam-treated wood [18,37,38]. The superheated steam treatment under 0.3 MPa increased the cellulose crystalline length of surface densified wood by 2.91%, which is higher than 0.1 MPa superheated steam-treated wood (1.18%). The increase of the cellulose crystalline length may be caused by the rearrangement of amorphous cellulose during the superheated steam treatment. The statistical results indicated no significant difference in the CrI between the untreated and 0.1 MPa superheated steam-treated wood but a significant difference between 0.3 MPa superheated steam-treated wood and the other two groups. This result indicated that 0.3 MPa superheated steam had a significant effect on the cellulose crystalline parameters of the surface densified wood.

Table 1. Cellulose crystalline parameters of surface densified wood with and without superheated steam treatment. Different letters within a column indicate significant differences ($p < 0.05$).

Treatment	CrI (%)	Crystalline Thickness (nm)	Crystalline Length (nm)
Untreated	43.31 b	2.71 b	20.28 b
0.1 MPa SHT	44.14 b	3.53 a	20.52 ab
0.3 MPa SHT	46.78 a	3.81 a	20.87 a

3.4. Elastic Modulus and Hardness of Cell Wall

Typical indentation load-depth curves of the wood cell wall are shown in Figure 6a. It can be observed that the surface densified wood with and without superheated steam treatment significantly displays different micromechanical behavior. Under the same experimental conditions, the reached peak depths of NI contact before unloading for untreated, 0.1 MPa, and 0.3 MPa superheated steam-treated wood specimens are 144.72, 131.09, and 113.75 nm, respectively, indicating that the superheated steam-treated wood with lower peak depths has higher mechanical properties than those of the untreated wood. These results are consistent with previous literature data [27].

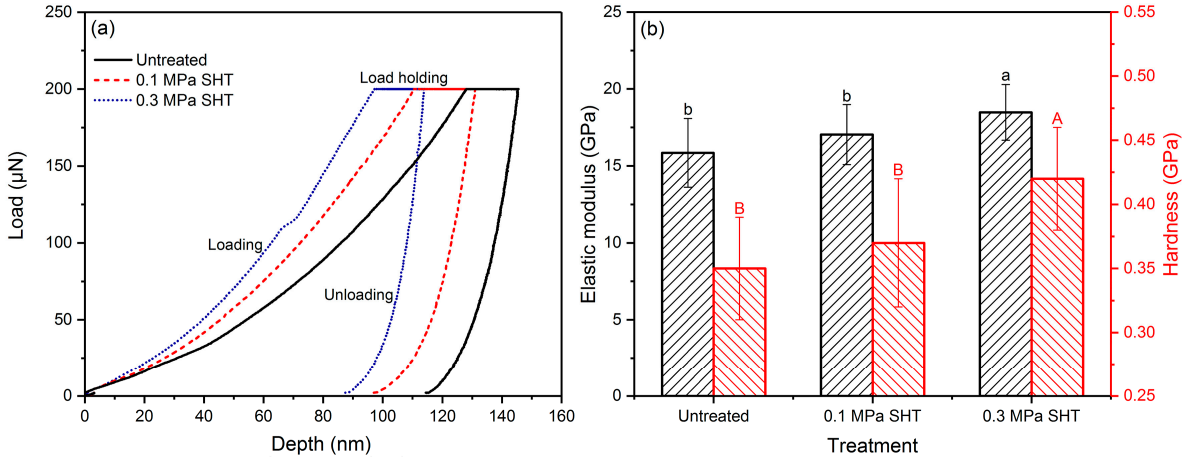

Figure 6. Changes in the load-depth curve (**a**), elastic modulus, and hardness of surface densified wood with and without superheated steam treatment (**b**).

The S2 layer accounts for 80% of the fiber cell wall thickness and is the main contributor to the mechanical properties of a single fiber. The nanoindentation measurements of the fiber cell wall mechanical properties are presented in Figure 6b. The average values of

the elastic modulus and the hardness of the untreated wood are 15.85 GPa and 0.35 GPa, respectively. Compared with untreated wood, the elastic modulus and hardness of 0.1 MPa superheated steam-treated wood were increased by 7.44% and 5.71%, respectively, but the differences were not statistically significant. The increase of elastic modulus and hardness of 0.3 MPa superheated steam-treated wood were 18.93% and 20.00%, respectively, which were significantly higher than that of untreated wood and 0.1 MPa superheated steam-treated wood. This indicates that superheated steam treatment at 0.1 MPa and 0.3 MPa has a reinforcement effect on the mechanical properties of fiber cell walls. When the heat treatment temperature was lower than 200 °C, the elastic modulus and hardness of *L. gmelinii* [23] and *moso* bamboo (*Phyllostachys pubescens*) [28] increased with the increase of heat treatment intensity, which was consistent with the results in this study. The mechanical properties of the wood cell wall are affected by chemical composition, the crystalline structure of cellulose, and moisture content [39–41]. The above ATR-FTIR and XRD results showed that the hemicelluloses acetyl group was broken after superheated steam treatment at 180 °C, and the cellulose amorphous zone was degraded, which increased the relative crystallinity of the cellulose, thus improving the stiffness of the wood cell wall. Moreover, the degree of hemicelluloses degradation reaction and the CrI of the 0.3 MPa superheated steam-treated wood are obviously higher than those of 0.1 MPa superheated steam-treated wood, which are consistent with the results of the elastic modulus and hardness. After superheated steam treatment at 0.1 MPa and 0.3 MPa, although some micro-cracks appeared on the fiber cell wall, the elastic modulus and hardness of the fiber cell wall increased significantly, indicating that the appearance of micro-cracks in the cell wall does not affect the elastic modulus and hardness of the fiber cell wall.

3.5. Creep Behaviours of Cell Wall

The creep ratio C_i and creep compliance $J(t)$ of the fiber cell wall were calculated by analyzing the loading holding segment data recorded by nanoindentation (Figure 7). Significant differences were observed in the creep behavior of the fiber cell wall between untreated and treated wood during the 200 μN peak loading force. As illustrated in Figure 7a, the creep ratio decreased markedly with superheated steam treatment. Compared with the untreated wood, 0.1 MPa and 0.3 MPa superheated steam-treated wood specimens exhibited 6.93% and 41.59% reduction in creep ratio, respectively. This is consistent with a previous study on the creep rate of *L. gemlinii* after heat treatment [23]. The results above illustrated that superheated steam treatment has positive effects on increasing the creep resistance of the wood cell wall under certain conditions.

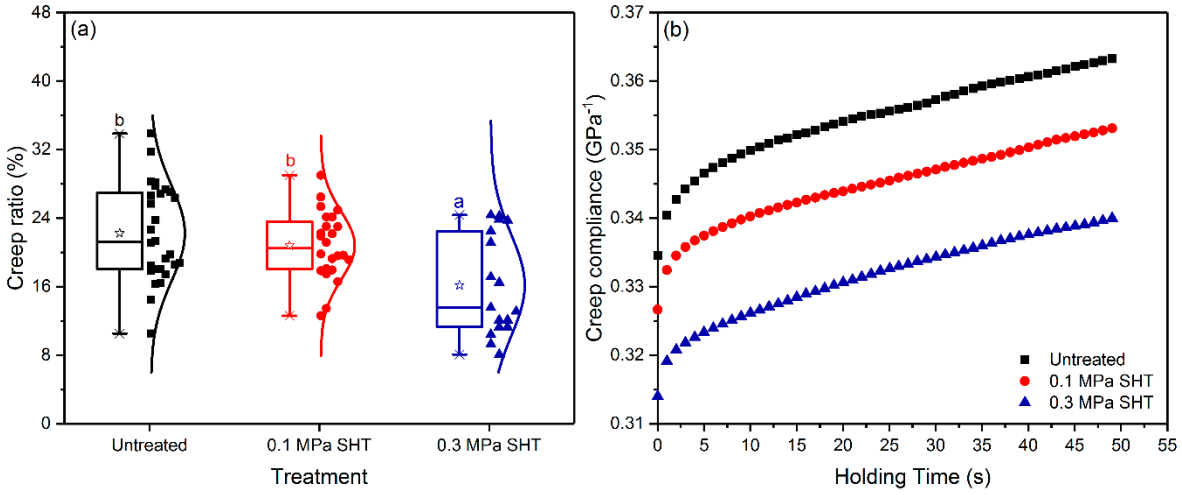

Figure 7. Changes of creep ratio (**a**) and creep compliance (**b**) of surface densified wood with and without superheated steam treatment.

Figure 7b shows the creep compliances of surface densified wood with and without superheated steam treatment. The variation of the time-creep compliance curve of untreated wood specimens was similar to that of treated wood specimens under 200 μN peak loading force. The creep compliance of the specimens displayed a dramatic increase in the first 5 s and then gradually slowed down with the extension of time. At room temperate, all test specimens have lower creep compliance values because the main components of wood are in the glassy state [26]. At the end of the loading-holding period, the maximum creep compliance J(50) of the cell walls in untreated wood was 0.363 GPa^{-1}. Compared with untreated wood, the maximum creep compliance J(50) of 0.1 MPa and 0.3 MPa superheated steam-treated wood was reduced by 2.83% and 6.76%, respectively, meaning that superheated steam treatment enhanced the resistance of the wood cell walls to creep. Microfilament angle, chemical component and activation energy are the main factors affecting the creep behavior of the wood cell wall [42]. The CrI, crystalline thickness, and crystalline length of surface densified wood increase significantly after superheated steam treatment, which strengthens the arrangement of cellulose molecular chains and increases the resistance of the wood cell wall to creep [18,21,37].

The experimental data of the creep test were fitted with a four-component Burger's model. In Figure 8, the black diamond represents the actual test data of creep compliance by nanoindentation in the indentation load-holding segment, and the red curves represent the creep compliance data fitted by the Burger's model. The correlation coefficients between the actual data and the fit exceeded the value of 0.99, indicating that Burger's model was suitable for predicting the creep behavior of surface densified wood with and without superheated steam treatment. The parameters in Burger's model include the modulus of elasticity (E_e), modulus of viscoelasticity (E_d), coefficients of plasticity (η_1), and viscoelastic parameter (η_2), as listed in Table 2. Superheated steam treatment resulted in a slight increase of E_e, η_1, and E_d. The increase of E_e represents the increased ability to resist deformation for surfaced densified wood, and the increase of η_1 represents increased plasticity [21]. Our previous study reported that the set recovery of densified wood decreased markedly after superheated steam treatment [17,18]. From a mechanical property perspective, the decrease of the set recovery of densified wood might be associated with increased plasticity during superheated steam treatment.

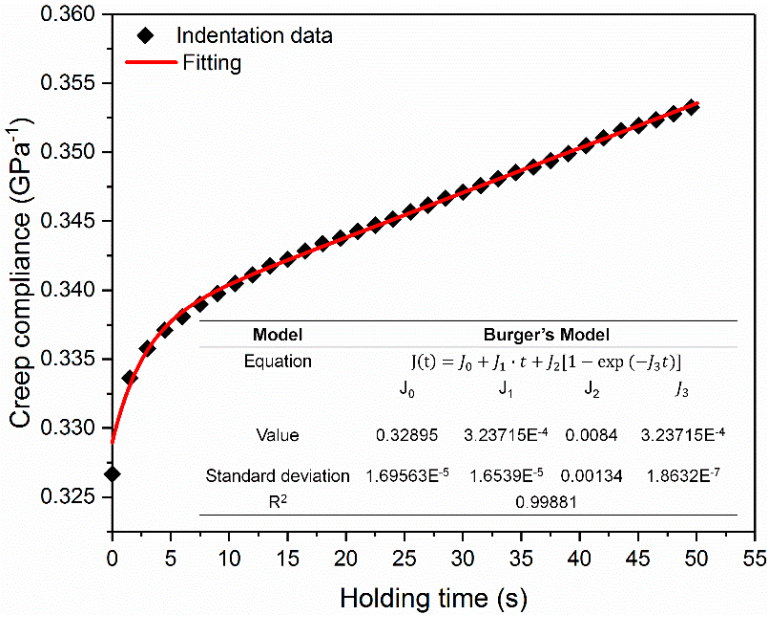

Figure 8. Representative fit curve of Burger's model to the load-holding segment of the nanoindentation curve.

Table 2. Elastic and viscosity coefficients from Burger's fit curves (maximum load: 200 μN; loading time: 50 s).

Treatment	Burger's Model					Mathematical Expression of Burger's Model
	E_e	η_1	η_2	E_d	R^2	
Untreated	2.97	3036.55	342.65	97.18	0.9985	$Y(t) = 0.3371 + 0.010 \times (1 - e^{-0.28362 \times t}) + 3.29 \times 10^{-4} \times t)$
0.1 MPa SHT	3.04	3089.13	315.37	119.05	0.9988	$Y(t) = 0.32895 + 0.008 \times (1 - e^{-0.37749 \times t}) + 3.24 \times 10^{-4} \times t)$
0.3 MPa SHT	3.15	3096.59	886.45	145.14	0.9969	$Y(t) = 0.3176 + 0.007 \times (1 - e^{-0.16373 \times t}) + 3.23 \times 10^{-4} \times t)$

4. Conclusions

This study investigated the effect of 0.1 MPa and 0.3 MPa superheated steam treatment on the microstructure, chemical composition, cellulose crystalline structure, and micromechanical properties of surface densified wood. Both 0.1 MPa and 0.3 MPa superheated steam treatments increased the elastic modulus and hardness of fiber cell walls in the surface densified wood, and the maximal increases were 18.93% and 20.00% for 0.3 MPa superheated steam-treated wood, respectively. However, the average creep ratio and maximum creep compliance J(50) of surface densified wood under 0.3 MPa decreased by 41.59% and 6.76%, respectively, compared with the untreated wood. Burger's model fitted the experimental data satisfactorily. The 0.3 MPa superheated steam treatment displayed a better effect on the enhancement of the elastic modulus, hardness, and creep resistance of the fiber cell wall than the 0.1 MPa superheated steam treatment. Superheated steam treatment at 0.1 MPa and 0.3 MPa resulted in micro-cracks appearing on the fiber cell walls, hemicelluloses degradation, and the CrI and crystalline size of cellulose increased. In summary, the superheated steam treatment could improve the elastic modulus, hardness and creep resistance of the fiber cell wall in surfaced densified wood by increasing the CrI and crystalline size, which is beneficial to maintaining the dimensional stability of surface densified wood.

Author Contributions: E.X.: investigation, formal analysis, data curation, writing—original draft. R.H.: funding acquisition, project administration, supervision. S.Y.: software, resources. All authors have read and agreed to the published version of the manuscript.

Funding: This research was funded by the Nature Science Foundation of China (Grant Nos. 32071690; 31670557).

Data Availability Statement: The data used to support the findings of this study are available from the corresponding author upon request.

Conflicts of Interest: The authors declare no conflict of interest.

References

1. Research Institute of Wood Industry. *Wood Physical and Mechanical Properties of Main Tree Species in China*; Forestry Publishing House: Beijing, China, 1982.
2. Chen, C.; Tu, D.; Zhou, Q.; Zhou, J.; Wang, X.; Cherdchim, B.; Ou, R. Development and evaluation of a surface-densified wood composite with an asymmetric structure. *Constr. Build. Mater.* **2020**, *242*, 118007. [CrossRef]
3. Laine, K.; Rautkari, L.; Hughes, M.; Kutnar, A. Reducing the set-recovery of surface densified solid Scots pine wood by hydrothermal post-treatment. *Eur. J. Wood Wood Prod.* **2013**, *71*, 17–23. [CrossRef]
4. Rautkari, L.; Properzi, M.; Pichelin, F.; Hughes, M. Properties and set-recovery of surface densified Norway spruce and European beech. *Wood Sci. Technol.* **2010**, *44*, 679–691. [CrossRef]
5. Belt, T.; Rautkari, L.; Laine, K.; Hill, C.A.S. Cupping behaviour of surface densified Scots pine wood: The effect of process parameters and correlation with density profile characteristics. *J. Mater. Sci.* **2013**, *48*, 6426–6430. [CrossRef]
6. Rautkari, L.; Laine, K.; Laflin, N.; Hughes, M. Surface modification of Scots pine: The effect of process parameters on the through thickness density profile. *J. Mater. Sci.* **2011**, *46*, 4780–4786. [CrossRef]
7. Navi, P.; Heger, F. Combined densification and thermo-hydro-mechanical processing of wood. *MRS Bull.* **2004**, *29*, 332–336. [CrossRef]
8. Laine, K.; Segerholm, K.; Wålinder, M.; Rautkari, L.; Hughes, M. Wood densification and thermal modification: Hardness, set-recovery and micromorphology. *Wood Sci. Technol.* **2016**, *50*, 883–894. [CrossRef]
9. Biziks, V.; Bicke, S.; Militz, H. Penetration depth of phenol-formaldehyde (PF) resin into beech wood studied by light microscopy. *Wood Sci. Technol.* **2019**, *53*, 165–176. [CrossRef]

10. Lykidis, C.; Kotrotsiou, K.; Tsichlakis, A. Reducing set-recovery of compressively densified poplar wood by impregnation–modification with melamine–formaldehyde resin. *Wood Mater. Sci. Eng.* **2019**, *15*, 269–277. [CrossRef]
11. Buchelt, B.; Dietrich, T.; Wagenführ, A. Testing of set recovery of unmodified and furfurylated densified wood by means of water storage and alternating climate tests. *Holzforschung* **2014**, *68*, 23–28. [CrossRef]
12. Pfriem, A.; Dietrich, T.; Buchelt, B. Furfuryl alcohol impregnation for improved plasticization and fixation during the densification of wood. *Holzforschung* **2012**, *66*, 215–218. [CrossRef]
13. Popescu, M.-C.; Lisa, G.; Froidevaux, J.; Navi, P.; Popescu, C.-M. Evaluation of the thermal stability and set recovery of thermo-hydro-mechanically treated lime (*Tilia cordata*) wood. *Wood Sci. Technol.* **2014**, *48*, 85–97. [CrossRef]
14. Inoue, M.; Kadokawa, N.; Nishio, J.; Norimoto, M. Permanent fixation of compressive deformation by hygro-thermal treatment using moisture in wood. *Wood Res. Tech. Notes* **1993**, *29*, 54–61.
15. Rautkari, L.; Honkanen, J.; Hill, C.A.S.; Ridley-Ellis, D.; Hughes, M. Mechanical and physical properties of thermally modified Scots pine wood in high pressure reactor under saturated steam at 120, 150 and 180 °C. *Eur. J. Wood Wood Prod.* **2014**, *72*, 33–41. [CrossRef]
16. Kutnar, A.; Kamke, F.A. Compression of wood under saturated steam, superheated steam, and transient conditions at 150 °C, 160 °C, and 170 °C. *Wood Sci. Technol.* **2010**, *46*, 73–88. [CrossRef]
17. Gao, Z.; Huang, R.; Chang, J.; Li, R.; Wu, Y. Effects of pressurized superheated-steam heat treatment on set recovery and mechanical properties of surface-compressed Wood. *Bioresources* **2019**, *14*, 1718–1730.
18. Xiang, E.; Feng, S.; Yang, S.; Huang, R. Sandwich compression of wood: Effect of superheated steam treatment on sandwich compression fixation and its mechanisms. *Wood Sci. Technol.* **2020**, *54*, 1529–1549. [CrossRef]
19. Ding, T.; Gu, L.; Li, T. Influence of steam pressure on physical and mechanical properties of heat-treated Mongolian pine lumber. *Eur. J. Wood Wood Prod.* **2011**, *69*, 121–126. [CrossRef]
20. Gao, Z.; Huang, R.; Chang, J.; Li, R.; Wu, Y.; Wang, Y. Sandwich compression of wood: Effects of preheating time and moisture distribution on the formation of compressed layer(s). *Eur. J. Wood Wood Prod.* **2019**, *77*, 219–227. [CrossRef]
21. Meng, Y.; Xia, Y.; Young, T.M.; Cai, Z.; Wang, S. Viscoelasticity of wood cell walls with different moisture content as measured by nanoindentation. *RSC Adv.* **2015**, *5*, 47538–47547. [CrossRef]
22. Wang, D.; Lin, L.; Fu, F. The difference of creep compliance for wood cell wall CML and secondary S2 layer by nanoindentation. *Mech. Time Depend. Mater.* **2019**, *9*, 1–12. [CrossRef]
23. Xing, D.; Li, J.; Wang, X.; Wang, S. In situ measurement of heat-treated wood cell wall at elevated temperature by nanoindentation. *Ind. Crop. Prod.* **2016**, *87*, 142–149. [CrossRef]
24. Engelund, E.T.; Svensson, S. Modelling time-dependent mechanical behaviour of softwood using deformation kinetics. *Holzforschung* **2011**, *65*, 231–237. [CrossRef]
25. Roszyk, E.; Mania, P.; Moliński, W. The influence of microfibril angle on creep of Scotch pine wood under tensile stress along the grains. *Wood Res.* **2012**, *57*, 347–358.
26. Wang, J.; Zhao, G. Creep of compressed wood of Chinese fir heat treated in air. *J. Beijing For. Univ.* **2002**, *24*, 52–58.
27. Wang, X.; Deng, Y.; Wang, S.; Min, C.; Meng, Y.; Pham, T.; Ying, Y. Evaluation of the effects of compression combined with heat treatment by nanoindentation (NI) of poplar cell walls. *Holzforschung* **2014**, *68*, 167–173. [CrossRef]
28. Li, Y.; Huang, C.; Li, W.; Wang, S.; Wang, X. The effects of thermal treatment on the nanomechanical behaviour of bamboo (*Phyllostachys pubescens* Mazel ex H. de Lehaie) cell walls observed by nanoindentation, XRD, and wet chemistry. *Holzforschung* **2017**, *71*, 129–135. [CrossRef]
29. Zhang, T.; Bai, S.; Zhang, Y.; Thibaut, B. Viscoelastic properties of wood materials characterized by nanoindentation experiments. *Wood Sci. Technol.* **2011**, *46*, 1003–1016. [CrossRef]
30. Li, R.; Gao, Z.; Feng, S.; Chang, J.; Wu, Y.; Huang, R. Effects of preheating temperatures on the formation of sandwich compression and density distribution in the compressed wood. *J. Wood Sci.* **2018**, *64*, 751–757. [CrossRef]
31. Segal, L.; Creely, J.J.; Martin, A.E.; Conrad, C.M. An empirical method for estimating the degree of crystallinity of native cellulose using the X-ray difractometer. *Text. Res. J.* **1959**, *29*, 786–794. [CrossRef]
32. Wei, L.; McDonald, A.G.; Stark, N.M. Grafting of bacterial polyhydroxybutyrate (PHB) onto cellulose via in situ reactive extrusion with dicumyl peroxide. *Biomacromolecules* **2015**, *16*, 1040–1049. [CrossRef]
33. Oliver, W.C.; Pharr, G.M. An improved technique for determining hardness and elastic modulus using load and displacement sensing indentation experiments. *J. Mater. Res.* **1992**, *7*, 1564–1583. [CrossRef]
34. Wei, X.; Tao, D.; Sheng, X.; Zhang, M. Modification of poplar wood using polyhexahydrotriazine and its effect on hygroscopicity. *J. Wood Chem. Technol.* **2018**, *38*, 214–223. [CrossRef]
35. Yin, Y.; Berglund, L.; Salmén, L. Effect of steam treatment on the properties of wood cell wall. *Biomacromolecules* **2011**, *12*, 194–202. [CrossRef] [PubMed]
36. Guo, J.; Song, K.; Salmén, L.; Yin, Y. Changes of wood cell walls in response to hygro-mechanical steam treatment. *Carbohydr. Polym.* **2015**, *115*, 207–214. [CrossRef]
37. Guo, J.; Rennhofer, H.; Yin, Y.; Lichtenegger, H.C. The influence of thermo-hygro-mechanical treatment on the micro- and nanoscale architecture of wood cell walls using small- and wide-angle X-ray scattering. *Cellulose* **2016**, *23*, 2325–2340. [CrossRef]
38. Yin, J.; Yuan, T.; Lu, Y.; Song, K.; Li, H.; Zhao, G.; Yin, Y. Effect of compression combined with steam treatment on the porosity, chemical compositon and cellulose crystalline structure of wood cell walls. *Carbohydr. Polym.* **2017**, *155*, 163–172. [CrossRef]

39. Stanzl-Tschegg, S.; Beikircher, W.; Loidl, D. Comparison of mechanical properties of thermally modified wood at growth ring and cell wall level by means of instrumented indentation tests. *Holzforschung* **2009**, *63*, 443–448. [CrossRef]
40. Wang, X.; Li, Y.; Deng, Y.; Yu, W.; Xie, X.; Wang, S. Contributions of basic chemical components to the mechanical behaviour of wood fiber cell walls as evaluated by nanoindentation. *Bioresources* **2016**, *11*, 6026–6039. [CrossRef]
41. Yu, Y.; Fei, B.; Wang, H.; Tian, G. Longitudinal mechanical properties of cell wall of Masson pine (Pinus massoniana Lamb) as related to moisture content: A nanoindentation study. *Holzforschung* **2011**, *65*, 121–126. [CrossRef]
42. Gril, J.; Hunt, D.; Thibaut, B. Using wood creep data to discuss the contribution of cell-wall reinforcing material. *Comptes Rendus Biol.* **2004**, *327*, 881–888. [CrossRef]